Chinese Chemical Letters 31 (2020) 2133–2136

Contents lists available at ScienceDirect

Chinese Chemical Letters

journal homepage: www.elsevier.com/locate/cclet

Communication

In-situ growth of V_2O_5 flower-like structures on ceramic tubes and their trimethylamine sensing properties

Dan Meng[a], Jianpeng Si[a], Mingyue Wang[b], Guosheng Wang[a], Yanbai Shen[c], Xiaoguang San[a,*], Fanli Meng[d,*]

[a] College of Chemical Engineering, Shenyang University of Chemical Technology, Shenyang 110142, China
[b] School of Chemical Engineering and Technology, Tianjin University, Tianjin 300072, China
[c] College of Resources and Civil Engineering, Northeastern University, Shenyang 110819, China
[d] College of Information Science and Engineering, Northeastern University, Shenyang 110819, China

ARTICLE INFO

Article history:
Received 12 October 2019
Received in revised form 1 December 2019
Accepted 12 December 2019
Available online 12 December 2019

Keywords:
In-situ growth
V_2O_5
Flower-like structures
Gas sensors
TMA

ABSTRACT

V_2O_5 flower-like structures assembled by thin nanosheets were *in-situ* growth on ceramic tubes by hydrothermal process. The structural characterization indicates that V_2O_5 flower-like structures is orthogonal diamond phase, which entirely covered on the surface of ceramic tubes. TMA sensing measured results revealed that the sensor based on V_2O_5 flower-like structures exhibited fast reversible and response, good selectivity to TMA and good stability at 200 °C. The good sensing performance may be ascribed to flower-like structures and directly growth sensing film on the ceramic tube without structure damage. Our works give a simple *in-situ* growth flower-like structures route on sensing device, which exhibits potential application for detecting trace amounts of TMA gas.

V_2O_5, as a typical n-type semiconducting metal oxide, has been proven to be the most attractive materials due to its high theoretical capacity, high surface energy, and pure orthorhombic structure [1], which has been widely used in catalysts [2], lithium-ion batteries [3], supercapacitor electrodes [4], electrochromic devices [5], *etc.* In order to improve their performances, multidimensional V_2O_5 structures such as nanowires [6], nanobelts [7], nanoneedles [8], 3D hierarchical architectures [9] and thin films [10] have been explored and fabricated in the past years, among which V_2O_5 hierarchical architectures assembled by nano-sized building blocks (particles, rods, sheets, *etc.*) have been the focus of considerable interest in recent years due to their unique physical and chemical properties. Benefiting from its unique structure characteristics, they are attractive for many important applications and exhibit a promising future.

Some reports in recent years have shown that V_2O_5 nanostructurs as a new type gas sensing material exhibited good sensing properties to various gases [8,11]. It is known that a relative large exposed area is favorable to improve the sensing performances [12]. Therefore, designing V_2O_5 hierarchical architectures with large surface area and high porosity is a promising approach for improving sensing performance. For achieving superior sensing performance, controllable synthesis of V_2O_5 with desirable nanostructures is a critical issue. Generally, during process of fabricating sensors, the sensing materials are coated on the electrode surface through using binders or additives. However, the sensing films easily drop from the electrode causing badly stability of gas sensors in the practical application. Hence, perfectly maintaining the well-designed V_2O_5 hierarchical architectures in the fabrication of sensing device process is important to obtain good sensing properties. Direct growth of V_2O_5 hierarchical architectures on electrode surface is an effective way to avoid the damage of well-designed structures during the process of fabrication sensing device, which could accelerate the integration of hierarchical architectures into sensing devices and improve the stability.

Trimethylamine (TMA) is widely used as organic solvent in the chemical industry, while there also exits non-negligible hazard to our human body [13]. Moreover, the TMA gas concentration can be used to monitor freshness degree of seafood and fish [14]. Hence, detecting TMA gas has attracted great attention to ensure the human health and safety of food. In this work, V_2O_5 flower-like structures were *in-situ* grown on the ceramic tube *via* a hydrothermal route and they exhibited good TMA sensing properties including fast response/recovery characteristics, good reproducibility and stability, and good selectivity, demonstrating potential application for detecting TMA gas.

* Corresponding authors.
E-mail addresses: sanxiaoguang@syuct.edu.cn (X. San), mengfanli@ise.neu.edu.cn (F. Meng).

https://doi.org/10.1016/j.cclet.2019.12.021

V_2O_5 flower-like structures were *in-situ* grown on the ceramic tube *via* a hydrothermal route. The experimental procedure is given in Scheme S1 (Supporting information). Initially, ammonium metavanadate (NH_4VO_3, 0.117 g) and polyvinylpyrrolidone (PVP, 0.1125 g) were dissolved in 15 mL distilled water and magnetically stirred at room temperature for 30 min. Subsequently, citric acid (0.315 g) was dissolved in 5 mL distilled water, and then added into the above solution dropwise under magnetic stirring until a bright yellow solution was formed. Then the solution was transferred to 50 mL Teflon-lined stainless autoclave. The ceramic tube which was cleaned by acetone, ethanol, and distilled water, respectively, was put into the bottom of autoclave. The autoclave was kept in an oven at 180 °C for required times (4, 8, 12 and 16 h), and then cooled down to room temperature. Thus, a layer of black product was deposited on the surface of the ceramic tube, which was washed several times with ethanol and distilled water, and dried under vacuum at 60 °C for 4 h. Finally, V_2O_5 flower-like structures were obtained by calcining the ceramic tube in a muffle furnace at 450 °C in air for 2 h. The final products synthesized at different hydrothermal reaction times (4, 8, 12 and 16 h) are denoted as sample 4h-V_2O_5, 8h-V_2O_5, 12h-V_2O_5, 16h-V_2O_5. The V_2O_5 flower-like structures were also prepared by hydrothermal route at 180 °C for 12 h. The structures of the products were characterized by X-ray diffraction (XRD, Shimadzu XRD-6100), field emission scanning electron microscope (FESEM, JEOL JSM-6700 F), transmission electron microscopy (TEM, JEOL EM002B) and X-ray photoelectron spectroscopy (XPS, Escalab 250Xi). The gas sensing properties were tested on a commercially available WS-30A static analysis system (Winsen Electronics Co., Ltd., Henan Province, China).

The FESEM images of the as-deposited products synthesized at 180 °C for 12 h are shown in Fig. S1 (Supporting information). The low magnification image (Fig. S1a) indicates that the products composed of flower-like structures with a diameter ranging from 1 to 3 μm. The overall image of ceramic tube as inset of Fig. S1a indicated that V_2O_5 flower-like structures entirely cover on the surface of the ceramic tube. Further observation (Figs. S1b and c) shows these flower-like structures are constructed by the nanosheets with a uniform thickness of about 20 nm. It is interesting that the V_2O_5 layer completely occupy the surface of the ceramic tube and the V_2O_5 flower-like structures composed of nanosheets are perfectly retained after calcining treatment (Figs. S2a-c in Supporting information), indicating the structural stability feature. Moreover, the diameter of V_2O_5 flower-like structures is also unchanged. This kind of structure is in favor of reducing the agglomeration between nanosheets, increasing the specific surface area and the stable of materials, thus enhancing the sensing properties. From the XRD patterns (Fig. S3 in Supporting information), it could observe that the precursor is the compounds of $V_2O_5{\cdot}3H_2O$ (JPCDS No. 07-0332), V_6O_{13} (JPCDS No. 19-1399) and VO_2 (JPCDS No. 09-0142), indicating that the precursor was incomplete oxidation and there exist multivalent V^{n+}, such as V^{5+} and V^{4+}. After calcining at 450 °C for 2 h, all of the diffraction peaks perfectly indexed to orthogonal diamond V_2O_5 phase (JPCDS No. 41-1426). In addition, no other characteristic peaks for impurities are observed, suggesting that the precursor is entirely converted in to V_2O_5 following the calcinations step. The peaks are strong and narrow, indicating the good crystallinity of the products.

The corresponding TEM image of the calcined products synthesized at 180 °C for 12 h is shown in Fig. S4a (Supporting information). It demonstrates that the central region of the flower-like structures is solid, and the edges show saw-tooth shape. The crystal lattice fringes could be obviously observed from a high-resolution image shown in Fig. S4b (Supporting information). The interplanar distances of 0.44 nm is close to the spacing of the (001) plane of the orthogonal V_2O_5. In order to prove the existence of the V and O element, XPS survey was performed for the calcined products synthesized at 180 °C for 12 h. Three elements (V, O and C) are observed from the full-wide scanned spectrum (Fig. S4c in Supporting information) and no other element peaks are observed, suggesting good purity of the products. According to Fig. S4d (Supporting information), two representative peaks around at binding energy values of 517.83 eV and 525.43 eV could be assigned to V $2p_{2/3}$ and V $2p_{1/2}$, respectively, corresponding to the V^{5+} from V_2O_5 phase [8,10]. The O 1s peak appearing at 530.63 eV could be ascribed to divalent oxygen. The above observations confirm the existence of V_2O_5.

To reveal the possible growth mechanism of V_2O_5 flower-like structures, the study of the morphological evolution of products with different reaction time has been conducted at 180 °C, as shown in Fig. 1. After hydrothermal reaction carrying out for 4 h, numerous of irregular cubic-like nanostructures with diameter about 100–200 nm were obtained, as shown in Fig. 1a. Some of them aggregated to spherical structures. Further lengthening the reaction time to 8 h, flower-like structures with diameter about 300–500 nm were formed, as shown in Fig. 1b. It also indicates that the flower petals are intersectional nanosheets with thickness of about 20 nm, which are loosely lapped over each other. As extending reaction time to 12 h, the diameter of flower-like structures significantly increases from 300–500 nm to 1–3 μm, as shown in Fig. 1c. The nanosheets of that constituting the flower-like structures grow up too, while the thickness of them is unchanged. As the reaction time is further extended to 16 h, the products remain the flower-like structures, while some of flowers begin to broken, as shown in Fig. 1d. There are also many irregular nanoblocks and nanosheets in the products and some of them accumulate with each other forming large idealized structures.

The above observations indicate that the reaction time affects the formation of V_2O_5 product morphology. The formation of V_2O_5 flower-like structures may be attributed to "reproduction mechanism" [15,16]. Here, NH_4VO_3 was used as vanadium source, which could dissociate NH_4^+ and VO_3^- ions in deionized water. Citric acid could produce H^+, thus, V_2O_5 ($V_2O_5{\cdot}nH_2O$) was formed. The formula is as follows (Eqs. 1 and 2) [17]:

$$NH_4VO_3 \rightarrow NH_4^+ + VO_3^- \quad (1)$$

$$2VO_3^- + 2H^+ \rightarrow V_2O_5 + H_2O \quad (2)$$

From XRD patterns (Fig. S2), it demonstrated that V_6O_{13}, VO_2 were also obtained, which indicated that citric acid not only

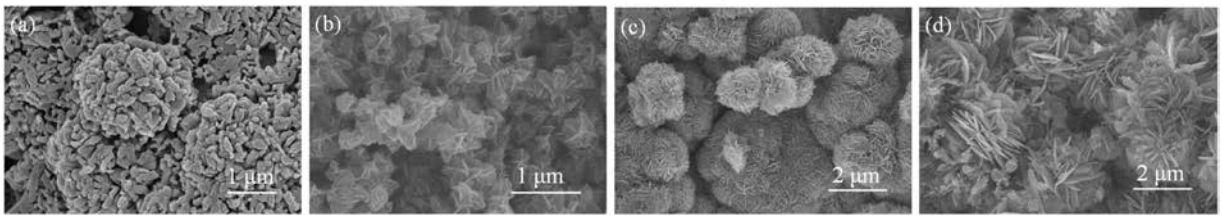

Fig. 1. FESEM images the calcined products synthesized at 180 °C for different reaction times: (a) 4 h, (b) 8 h, (c) 12 h and (d) 16 h.

provides H^+ for reactions but also as the reducing agent for reducing NH_4VO_3 [18]. Because some of V^{5+} was reduced to V^{4+}, VO_3^- ions form new aggregates of multivalent V, such as V_2O_5, V_6O_{13}, VO_2. During the hydrothermal process, vanadium oxide nucleates could be primarily formed on the surface of the ceramic tube. Citric acid owns three carboxylic (–COOH) functional groups, which could form coordination complex on the surfaces of V_nO_m crystal nucleus [18–20]. Therefore, the growth direction and rate of different facets were affected effectively by binding to specific facets. Following by the crystal growth process, the vanadium oxide nucleates served as seeds and subsequently grow to thin nanosheets [15,16]. In addition, PVP was used and its templating nature promotes the thin nanosheets gradually self-oriented and assembled to flower-like hierarchical V_nO_m structures [21]. The shortened reaction time results in forming nanoparticles and stacked with each other forming large microspheres to reduce the surface energy during the cooling process of the autoclave. As the reaction progresses, the growth of the crystals slows down due to consuming vanadium ions and H^+, which is not enough for the growth of the initial nanosheets in the circumference. Extending the reaction time leads to enhancing grain growth and nucleation sites, thereby, increasing the nanosheets size. As further increasing the reaction time, some tiny irregular nanoparticles were formed and some of them attaced on the surface of V_nO_m flower-like structures or aggregated with each other forming large particles to decrease the surface energy. After calcining, these unstable oxides undergo deamination and are converted into a stable V^{5+} valence oxide.

The TMA sensing properties of V_2O_5 products were studied. The optimal operation temperature was obtained by testing these sensors from 100 °C to 400 °C. As shown in Fig. 2a, the response value of all sensors increases accompanied by increasing operating temperature, exhibiting the maximum value at 200–250 °C, then, it decreases with further increasing temperatures. This phenomenon can be explained by the balance between the gas adsorption-desorption rate and the movement of the adsorbed oxygen species [22,23]. Increasing temperature is in favor of the chemical adsorption of oxygen and TMA and thermal reactions between TMA molecules and surface adsorbed oxygen species. While, at temperature above the optimal operating temperature, the desorption rate of TMA gas was greater than adsorption, resulting in reduced response. The optimal operating temperature of 4h-V_2O_5 sensor is 250 °C, at which the corresponding maximal response is 1.31. While, the optimal operating temperatures of 8h-V_2O_5, 12h-V_2O_5 and 16h-V_2O_5 sensors are 200 °C, which are lower than that of 4h-V_2O_5 sensor, and the corresponding maximal responses are 1.63, 2.17 and 1.82, respectively. Obviously, 12h-V_2O_5 flower-like structures show higher response than that of other products. The selectivity is a very important factor for practical application. Therefore, the gas responses of sensors based on the 12h-V_2O_5 to 5 ppm of various target gases were measured at 200 °C, as displayed in Fig. 2b. It is obvious that the sensor exhibited the maximum response to TMA gas, indicating its good selective ability in the gas detection process. The good selectivity of the sensor could be ascribed to low C—N bond energy in TMA and high electron cloud density around N atom in TMA [24–26].

The transient dynamic resistance of 4h-V_2O_5 and 12h-V_2O_5 sensors to TMA gas in the contration range of 1–200 ppm TMA at 200 °C is shown in Fig. S5a (Supporting information). It is found that the sensor resistance decreases rapidly upon exposure TMA gas, and it quickly returns to the initial state after removing TMA gas. Both sensors show a typical behavior for the n-type semiconductor, that is, when the sensors expose to a reducing gas, such as TMA gas, the resistance decreases. The enlarged response transient curves exhibit in Fig. S5b (Supporting information). The response time (13 s) and recovery times (13 s) of the 12h-V_2O_5 sensor to 5 ppm TMA gas are shorter than that of the 4h-V_2O_5 sensor (20 s and 22 s, respectively). The fast responses and recovery characteristic of 12h-V_2O_5 sensor could be ascribed to the unique flower-like structures which facilitate a fast mass transfer of TMA molecules. This short response and recovery times are valuable for practical application. The response values of two sensors *versus* the TMA concentration at 200 °C is shown in Fig. S5c (Supporting information). Obviously, 12h-V_2O_5 sensor is more sensitive than the 4h-V_2O_5 sensor, and the response of 12h-V_2O_5 increase faster accompanied with the increase of gas concentration than that of 4h-V_2O_5 sensor. Such good dependence of response on the gas concentration indicates that 12h-V_2O_5 sensor has a wide detection range and is suitable for detecting TMA in the low concentration range.

The stability of the semiconductor gas sensor is also an important indicator in practical applications. The sensing response of the sensor based on *in-situ* growth V_2O_5 flower-like structures (12h-V_2O_5 sensor) and V_2O_5 flower-like structures which were coated on the ceramic tube (coated-sensor) to 5 ppm TMA was measured at 200 °C, as shown in Fig. 3. Evidently, the sensing response of 12h-V_2O_5 sensor is higher than that of coated-sensor. On the other hand, for the coated-sensor, the response decreased at first 20 days, and then slowly decreased. The change amplitude of the responses during the tested days was 17.7%. While, for the 12h-V_2O_5 sensor, there is little variation in the response for over 60 days, and the change amplitude of the responses was controlled within 11.1%. These results demonstrate that 12h-V_2O_5 sensor possesses not only high response, but also good long-term stability compared to coated-sensor. The good sensing performance of 12h-V_2O_5 sensor may be attributed to the *in-situ* growth sensing film which is not only remaining well-designed flower-like structures but also avoiding using binders. Moreover, the sensing response of 12h-V_2O_5 sensor to diffident TMA concentrations (5 ppm, 20 ppm and 100 ppm) was also measured at 200 °C, as shown in Fig. S6a (Supporting information). It observes that the sensor remains its

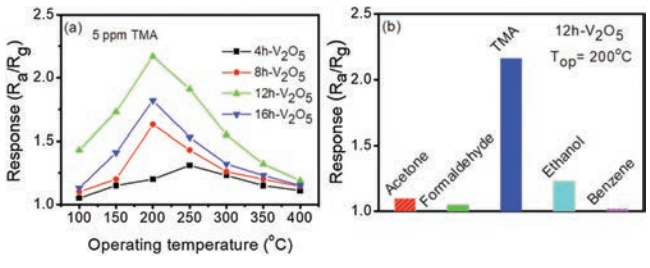

Fig. 2. (a) Temporal responses of the sensors made of V_2O_5 products upon exposure to 5 ppm TMA gas. (b) Selectivity of 12h-V_2O_5 sensor.

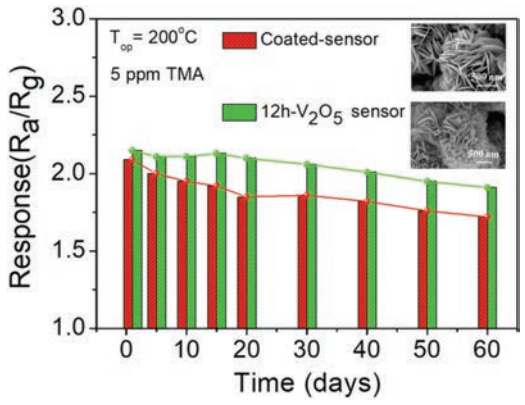

Fig. 3. Stability of the 12h-V_2O_5 sensor and coated-sensor at 200 °C.

response without obvious variation to TMA at different concentrations over the testing period, implying its good stability. In addition, the reproducibility of the 12h-V_2O_5 sensor was investigated by measuring 5 ppm TMA gas five times at 200 °C. From Fig. S6b (Supporting information), it is obvious that the response and recovery curves have no clear variation and the response is reproducible, indicating its good repeatability and stability for detecting TMA gas. It is concluded that the sensor based on V_2O_5 flower-like structures exhibits excellent TMA gas sensing performance, and it may have potential applications in monitoring TMA gas.

The metal oxide semiconductor sensor is attributed to the surface resistance control type, and the sensing response depends on the adsorption and desorption of gas molecules. A possible sensing mechanism is presented in Scheme S2 (Supporting information). As an n-type semiconductor, when V_2O_5 is in contact with oxygen, oxygen molecules are adsorbed on the surface of V_2O_5 and converted into adsorbed oxygen ions (O^-, O^{2-} or O_2^-) [27]. This electron capture process causes a depletion layer on the surface of V_2O_5, leading to a high resistance state. When V_2O_5 is exposed to TMA gas, these gas molecules react with surface oxygen ions as follows (Eqs. 3–5) [28]:

$$4N(CH_3)_3 + 21O_2^- \rightarrow 2N_2 + 18H_2O + 12CO_2 + 21e^- \quad (3)$$

$$2N(CH_3)_3 + 21O^- \rightarrow N_2 + 9H_2O + 6CO_2 + 21e^- \quad (4)$$

$$2N(CH_3)_3 + 21O^{2-} \rightarrow N_2 + 9H_2O + 6CO_2 + 42e^- \quad (5)$$

This process releases electrons back to V_2O_5, which causes an increase in charge concentration by electron-depletion layer recombination, resulting in a decrease in resistance. According to the definition of response ($S = R_a/R_g$), the larger changes in the resistance reflect higher response. In our work, flower-like hierarchical structures assembled by many thin nanosheets could offer more active sites for chemisorption of gases and its high porosity provides excellent channels for gas diffusion, benefiting for enhancing the sensing properties [29]. Moreover, directly growth flower-like hierarchical structures on the ceramic tube greatly increases stability.

In conclusion, V_2O_5 flower-like structures assembled by thin nanosheets were *in-situ* growth on ceramic tubes by hydrothermal process. The structural characterizations and TMA sensing properties were investigated. The V_2O_5 flower-like structures were entirely covered on the surface of the ceramic tube. TMA sensing measured results revealed that V_2O_5 flower-like structure sensor exhibited fast reversible and response, good selectivity to TMA and good stability. The good sensing performance may be ascribed to flower-like structures and directly growth sensing film on the ceramic tube without structure damage.

Declaration of competing interest

The authors declare that they have no known competing financial interests or personal relationships that could have appeared to influence the work reported in this paper.

Acknowledgments

This research work was financially supported by the National Natural Science Foundation of China (Nos. 61973223, 61673367 and 51674067) and Liao Ning Revitalization Talents Program (No. XLYC1807198).

Appendix A. Supplementary data

Supplementary material related to this article can be found, in the online version, at doi:https://doi.org/10.1016/j.cclet.2019.12.021.

References

[1] X.Y. Liu, J.H. Zeng, H.N. Yang, K. Zhou, D. Pan, RSC Adv. 8 (2018) 4014–4031.
[2] Y.L. Niu, Z. Xu, M. Li, et al., Chin. Chem. Lett. 19 (2008) 245–248.
[3] Y.W. Li, J.H. Yao, E. Uchaker, et al., J. Phys. Chem. C 117 (2013) 23507–23514.
[4] J.H. Xu, F. Zheng, H.Q. Gong, et al., Cryst. Eng. Comm. 19 (2017) 6412–6424.
[5] Y.N. Ko, S.H. Choi, Y.C. Kang, S.B. Park, ACS Appl. Mater. Interfaces 5 (2013) 3234–3240.
[6] B.Y. Yeh, B.S. Jian, G.J. Wang, W.J. Tseng, RSC Adv. 7 (2017) 49605–49612.
[7] W. Zeng, W.G. Chen, Z.Y. Li, et al., Mater. Res. Bull. 65 (2015) 157–162.
[8] S.A. Hakim, Y.L. Liu, G.S. Zakharova, W. Chen, RSC Adv. 5 (2015) 23489–23497.
[9] X.C. Ren, Y.J. Zhai, L. Zhu, et al., ACS Appl. Mater. Interfaces 8 (2016) 17205–17211.
[10] M. Epifani, T. Andreu, C.R. Magana, et al., Chem. Mater. 21 (2009) 1618–1626.
[11] R.B. Wang, S. Yang, R. Deng, et al., RSC Adv. 5 (2015) 41050–41058.
[12] X.W. Cheng, Y.H. Zhu, et al., Chin. Chem. Lett. 29 (2018) 405–416.
[13] Z.Q. Li, W.J. Wang, Z.C. Zhao, et al., RSC Adv. 7 (2017) 28366–28372.
[14] Y. Li, J.Q. Liu, J.J. Zhang, et al., Chin. Chem. Lett. (2019), doi:http://dx.doi.org/10.1016/j.cclet.2019.11.048.
[15] Y.H. Sun, P.P. Dong, X. Lang, J.M. Nan, Chin. Chem. Lett. 25 (2014) 915–918.
[16] C. Wang, R.Z. Sun, X. Li, et al., Sens. Actuator. B -Chem. 204 (2014) 224–230.
[17] X. Chen, X.M. Sun, Y.D. Li, Inorg. Chem. 41 (2002) 4524–4530.
[18] J.H. Xu, F. Zheng, H.Q. Gong, et al., Cryst. Eng. Comm. 19 (2017) 6412–6424.
[19] L.L. Guo, H. Chen, N.Y. He, Y. Deng, Chin. Chem. Lett. 29 (2018) 1829–1833.
[20] L.Q. Mai, C.S. Lao, B. Hu, et al., J. Phys. Chem. B 110 (2006) 18138–18141.
[21] E. Uchaker, N. Zhou, Y.W. Li, G.Z. Cao, J. Phys. Chem. C 117 (2013) 1621–1626.
[22] L.L. Wang, Z. Lou, R. Zhang, et al., ACS Appl. Mater. Interfaces 8 (2016) 6539–6545.
[23] J.R. Huang, L.Y. Wang, C.P. Gu, et al., Sens. Actuator. B -Chem. 207 (2015) 782–790.
[24] S. Zhang, P. Song, Z.B. Tian, Q. Wang, Mat. Sci. Semicon. Proc. 75 (2018) 58–64.
[25] V. Mounasamy, G.K. Mani, D. Ponnusamy, et al., New J. Chem. 43 (2019) 11069–11081.
[26] S. Yang, Y.L. Liu, W. Chen, et al., Sens. Actuator. B -Chem. 226 (2016) 478–485.
[27] W.C. Wang, F.Q. Liu, B. Wang, et al., Chin. Chem. Lett. 30 (2019) 1261–1265.
[28] D. Meng, D.Y. Liu, G.S. Wang, et al., Appl. Surf. Sci. 463 (2019) 348–356.
[29] N. Li, Y. Fan, Y. Shi, et al., Sens. Actuator. B -Chem. 294 (2019) 106–115.